Thesis for The Degree of Licentiate of Engineering

Identifying locally induced loads in hard rock tunnel linings by distributed optical fibre sensors

August Jansson

Department of Architecture and Civil Engineering
Chalmers University of Technology
Gothenburg, Sweden, 2024

Identifying locally induced loads in hard rock tunnel linings by distributed optical fibre sensors

August Jansson

Technical report: 2024:2
Lic/Architecture and Civil Engineering/Chalmers University of Technology

Department of Architecture and Civil Engineering
Division of Structural Engineering
Concrete Structures Research Group
Chalmers University of Technology
SE-412 96 Göteborg,
Sweden
Phone: +46(0)31 772 1000

Printed by Chalmers Digitaltryck,
Gothenburg, Sweden 2024.

Identifying locally induced loads in hard rock tunnel linings by distributed optical fibre sensors

August Jansson

Department of Architecture and Civil Engineering
Chalmers University of Technology

Abstract

In an infrastructure system, tunnels enable fast means of transportation in impassable terrain or city areas. However, inspections and maintenance can be expensive due to long down time and, in hard rock tunnels, the complexity of the structure may lead to over designing.

This thesis presents an experimental series aiming to reproduce loading conditions acting on shotcrete tunnel linings in hard rock. The specimens consisted of two concrete layers, a top fibre reinforced concrete layer simulating a shotcrete lining, and a 300 mm thick substrate layer simulating rock. The top FRC layer response was measured using strain sensing distributed optical fibre sensors (DOFS) installed in two layers. A full factorial design with four factors and two levels was applied, where the varied factors were load conditions, load size, lining thickness and tensile bond strength between lining and substrate.

From the experimental results, it is concluded that using DOFS to monitor loads in tunnel linings are suitable as the global behaviour is captured at low load magnitudes and that performance indicators, such as cracks, can be used to identify the load type.

The work presented is part of a research project aiming to develop a machine learning model, trained on synthetic data from finite element analyses calibrated with the acquired experimental results, to identify loads and predict the structural integrity of a tunnel lining. The experimental results will ultimately be used to verify the machine learning model and, thus, implications for future finite element and machine learning models are discussed based on the experimental results.

Keywords

Distributed optical fibre sensors, Tunnel lining experiments, Structural health monitoring

List of Publications

Appended publications

This thesis is based on the following publications:

[**Paper I**] **A. Jansson**, I. Fernandez, C. G. Berrocal, R. Rempling, *Investigation of the impact of concrete surface treatment methods on the interfacial bond strength*
SynerCrete 2023: International RILEM Conference on Synergising Expertise towards Sustainability and Robustness of Cement-based Materials and Concrete Structures, pp 925–934.

[**Paper II**] **A. Jansson**, A. Sjölander, I. Fernandez, C. G. Berrocal, R. Rempling, *Investigating the response of tunnel linings through distributed optical fiber sensing*
Submitted, under review.

[**Paper III**] **A. Jansson**, I. Fernandez, C. G. Berrocal, R. Rempling, *Strain distributions for shotcrete failure in hard rock tunnels*
IABSE Symposium Manchester 2024.

Other publications

The following publication was published during my PhD studies. However, it is not appended to this thesis, due to contents overlapping that of appended publications or contents not related to the thesis.

[**a**] **A. Jansson**, I. Fernandez, C. G. Berrocal, R. Rempling, *Experimental design for shotcrete tunnel lining with distributed optical fibre monitoring Proceedings of the XXIV NCR Symposium 2022.*

Acknowledgment

The research presented in this licentiate thesis was conducted during 2022 and 2023 at the division of Structural Engineering, Department of Civil and Architectural engineering at Chalmers University of Technology. The work was funded by the Swedish transport administration through BBT, grant number 2020-006, and I want to express my sincere gratitude the funder.

I want to thank my supervisors, Associate Professor Ignasi Fernandez, Senior Lecturer Carlos Gil Berrocal and Associate Professor Rasmus Rempling for their support and guidance during this work. I would also like to thank the laboratory engineers, Sebastian Almfeldt and Anders Karlsson for teaching and guiding me in the laboratory work as well as discussing experimental solutions. Further, I would like to thank all my colleagues at Chalmers university of Technology for supporting me and contributing to a nice working environment and thanks to my examiner Jelke Dijkstra for insights and guidance throughout this work.

Thanks also to Jennifer for all her support and love during this time and thanks to my family for encouraging me to pursue my interests.

Contents

Part I

Summary

Chapter 1

Introduction

1.1 Background

Shotcrete was introduced in tunnel linings in 1914, but it was not until 1955 that the wet mix method was first applied allowing for large scale usage of shotcrete in tunnel linings. Instead of mixing the concrete and water in the nozzle, known as the dry mix method, factory mixed concrete could be connected directly to the shotcrete hose and sprayed on the rock (Sjölander, 2020). In combination with shotcrete, rock bolts are often systematically drilled to fasten larger loose blocks to the underlying intact rock while the shotcrete lining carries smaller blocks and loose rock mass between the rock bolts.

Design of shotcrete varies depending on rock quality, density of faults and joints as well as the geometry of the tunnel. Empirical designs such as the Q-system and RMR are used in good quality rock with small amount of faults and applicable geometries (Barton et al., 1974). In other cases, detailed design using analytical or numerical models is carried out. In the latter, the loads acting on the linings are assumed as the largest possible and the residual capacity of the fibre reinforcement in the shotcrete is commonly used (Trafikverket, 2015).

In all tunnel construction, monitoring of rock displacements and convergence is crucial in determining tunnel stability and validating design assumptions. Common methods used today include total stations, inclinometers, strain gauges and lidar scanning (Hoult & Soga, 2014). However, no method for monitoring rock loads acting on the shotcrete lining exists today. Hence, the utilization rate of shotcrete linings is unknown which in turn may lead to unsafe or overdimensioned structures.

In recent research, distributed optical fibres sensors (DOFS) have been utilized to measure distributed strain profiles in tunnel linings (Monsberger & Lienhart, 2021). Results from those studies include methods for successfully measuring convergence and displacements in the lining due to deformations in the surrounding rock. The DOFS were installed in prefabricated reinforced

concrete linings for soft rock. Moreover, in Battista et al. (2015), DOFS were installed in clay tunnel sections sensitive to displacements from continued tunnel construction to ensure safe environments during construction. However, rock loads acting locally on tunnel linings in hard rock have not previously been measured and studied using DOFS. Furthermore, mainly long gauge DOFS have been applied in previous studies. By using shorter gauge lengths, the sensing range decrease drastically, but cracks and other local effects can be monitored (Berrocal et al., 2021). The increased resolution and detail of measurements can potentially be used to identify loading conditions and predict the structural integrity of the tunnel lining using advanced machine learning algorithms.

1.2 Purpose and objectives

The purpose of the work presented in this thesis is to experimentally identify rock loads acting on shotcrete tunnel linings in hard rock using DOFS. This thesis constitutes the first part of a research project and the following objectives defines the purpose of the thesis:

1. To identify and define performance indicators in shotcrete tunnel linings.
2. To show that advanced sensor-based monitoring systems are adequate tools for obtaining unique and trustworthy data in shotcrete tunnel linings.

The purpose of the research project is to investigate how DOFS can be used in combination with advanced statistical AI-models, trained on data generated with finite element models, to verify and predict the structural integrity of shotcrete tunnel linings in hard rock. The following objectives define the next part of the research project:

3. To demonstrate the suitability of FEA models, in combination with structural sensor data, as a foundation for training AI-tools.
4. To demonstrate how an AI-tool can be used as an advanced statistical model for the verification of performance indicators and prediction of how these are met during long service technical lives.

The research project objectives 3 and 4 are included in the thesis as they influence the experimental approach and the discussion section of the thesis.

1.3 Research methods

A flowchart depicting the research project is shown in Figure 1.1 and included in this thesis are the preliminary experiment, Paper 1, and the main tunnel experiment, Paper 2 and 3.

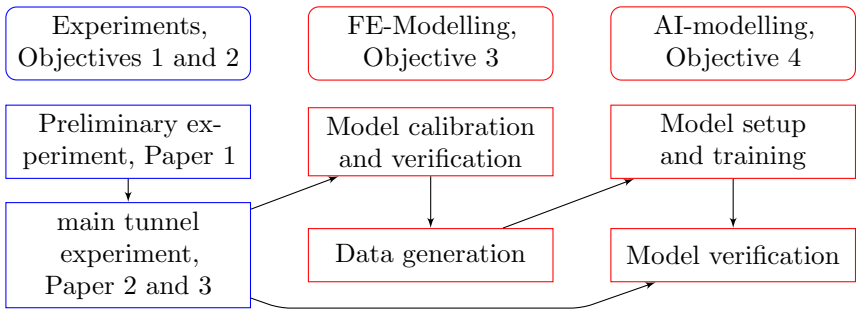

Figure 1.1: Research project main tasks and workflow. The experiments section is included in this thesis.

A preliminary experiment was conducted to investigate methods that affect the bond behaviour between two layers of separately cast concrete. The results were later implemented in the main tunnel load experiment which aimed to replicate local load types acting on tunnel linings. In the next stage of the research project, a FE-model will be implemented to simulate the lining behaviour, and through numerous simulations with varying inputs to the model, a database will be generated. The database will then be used to train a machine learning algorithm, which in the last part of the project it will be tested and verified using the experimentally acquired data. By applying an AI, trained on synthetically generated FEM data, that is able to detect load types and predict failure progression from measured data, costs for expensive experimental programs and in-situ testing can be decreased and real time structural verification can increase the structural safety.

1.4 Scope

The experiments presented in this thesis are designed to replicate the structural behaviour of a shotcrete tunnel lining with varying geometrical and material parameters: load type, load size, lining thickness and bond strength. The behaviour of rock bolts is, however, not investigated. The lining behaviour is investigated based on loads, while other strain inducing processes, e.g., shrinkage, are not considered. Furthermore, the usage of DOFS in tunnel linings will be investigated with respect to sensitivity, installation and precision. Moreover, improvements of design guidelines or building techniques are not considered in this work as input materials in the experiments are different from a real tunnel.

1.5 Limitations

Experimental work has been conducted in a laboratory, restricting the size and number of the experimental specimens. Maximum specimen weight due to lifting tools were 5 tonnes and the spacing between fastening points in the laboratory

strong floor were 1 m which limited the anchorage spacing. Furthermore, the material substitutions for shotcrete and rock to fibre reinforced concrete and plain concrete respectively, leads to deviations between the experimental results and a real tunnel case.

1.6 Thesis outline

This thesis consists of a five chapter introductory part and three appended papers.

Chapter 1 This chapter includes a brief background of the subject and introduces the purpose, scope and limitations of the thesis.

Chapter 2 The frame of reference for the study is presented.

Chapter 3 The experimental program is presented, including experimental approach, methods and data collection

Chapter 4 Main results from the appended papers are presented

Chapter 5 Discussion of results and implications to the research project

Chapter 6 Conclusions and future research are presented

1.7 Summary of included papers

Paper 1 Preliminary experiments on how to achieve a low non-zero and a high adhesive bond strength between two separately cast concrete layers are presented in this paper. To investigate how a low non-zero bond could be attained, different surface treatments were applied to a hardened concrete slab. After applying the surface treatment, another layer of concrete was cast on top of the treated concrete slab. It was concluded from literature that a hydro-demolition surface treatment yields a high bond strength and, from the conducted experiments, that a ground surface yields a low non-zero bond strength.

Paper 2 In this paper, loads acting on tunnel linings are simulated experimentally. A factorial design is implemented with four factors each of which had two levels, resulting in 16 specimens. The investigated factors were the loading condition, load size, lining thickness and bond strength. All specimens were instrumented with DOFS that measured distributed strains. The paper focuses on early strain measurements prior to the peak load and consequently the bond failure. Following the analysis of strain patterns, mechanical models were proposed describing the behaviour of the lining. Furthermore, the sensitivity of DOFS was investigated regarding the distance to the loaded zone.

Paper 3 The same experiments as in paper 2 are analysed in this paper, but with a focus on strains measured after the initial bond failure. It was shown that even though the bond strength has a small influence on the peak load, the residual capacity of hydro-demolished specimens is considerably higher than for ground specimens. The analysis showed that the residual capacity difference is attributed to different failure modes. In ground specimens, the lining is completely debonded from the substrate slab while the lining is only partly debonded in hydro-demolished specimens.

Chapter 2

Frame of reference

In this chapter, the applied frame of reference for the study is presented, which focus on the behaviour of shotcrete linings, distributed optical fibre sensors (DOFS) and FEM and AI modelling approaches.

2.1 Shotcrete tunnel linings in hard rock

In hard rock tunnels, global stability is usually achieved through arch action in the rock. However, due to existing faults and joints in the rock, a risk for fallouts of loose rock blocks and loose rock material exists. To mitigate this risk, larger rock blocks are secured to the overlaying rock using steel rock bolts and a layer of shotcrete is sprayed to carry smaller blocks or loose rock material between the rock bolts (Palmström & Stille, 2015).

The load carrying mechanisms of a shotcrete lining depends on several parameters. Most important, the load type and the state of the bond between shotcrete and rock, understanding bond as the normal stresses arising between the lining and rock, influence how loads are transferred from the lining to the overlying rock or rock bolt (Barrett & McCreath, 1995). External loads on the lining stemming from the surrounding rock can be classified into two types, (i) loose rock blocks and (ii) loose rock material. The former occurs due to intersecting faults in the rock which can form cone-formed loose blocks; the latter consists of several smaller rocks, or gravel, formed by degradation of the rock due to groundwater leakage, freeze and thaw cycles or deformations in the rock (Bernard & Thomas, 2020). For both load types, the bond conditions between shotcrete and rock affect the load carrying mechanisms. With an intact bond, loads are transferred through the bond to the rock, while a loss of bond results in loads being carried through the shotcrete lining to the rock bolts.

In analytic design of shotcrete linings, recommendations from the Swedish transport agency (Trafikverket, 2015) state that cases for both intact and absent bond should be considered for loose block loads and absent bond for loose rock material. However, even though both intact and absent bond are

considered in analytical design, a good bond is desirable and cores are systematically drilled and tested in tension during tunnel construction to verify sufficiently high bond strengths. Typically, the bond strength varies between 0 and 2 MPa and depends on both surface roughness and mineral composition of the rock (Hahn, 1983), but also on the cleanliness of the rock surface and the rock scaling method prior to shotcrete spraying (Malmgren et al., 2005).

In previously performed experiments (Fernandez-Delgado et al., 1975; Holmgren, 1987), the capacity of shotcrete linings was tested by spraying or casting a layer of concrete on top of three concrete or rock slabs placed in a line, securing the outer slabs with rock bolts, and pushing the middle slab upwards using a hydraulic jack. The results showed an initial high stiffness until bond failure between the shotcrete and outer slabs occurred and hinges formed at the middle slab edge and at the rock bolt. Lower load levels were still resisted through residual flexural capacity enabled by the steel fibre reinforcement in the shotcrete.

2.2 Monitoring of tunnels

In tunnel construction, monitoring is crucial for verifying design assumptions and ensuring safety for workers. Common techniques include, e.g., inclinometers, total stations and strain gauges, with the aim to control tunnel convergence, the displacement of blocks and faults, and stress and strains in the lining (Hoult & Soga, 2014). Furthermore, during the service life of a tunnel, regular inspections are required to ensure durability and safety. Cracks, leakages and other observable deterioration are visually inspected while non-visible defects, such as loss of bond between shotcrete and rock, are identified using other techniques. Loss of bond between rock and shotcrete can be detected using a hammer probing technique, where the inspector knocks on the wall and listens for hollow sounds, indicating a loss of bond. This method require tunnel down time for traffic and only provide qualitative results.

2.2.1 Distributed optical fibre sensors

The optical fibre sensing technology was first commercially used in the 1980s when optical time-domain reflectometry (OTDR) was invented to test optical fibres in the telecommunications industry and detect eventual breaks or defects in the fibre (Güemes & Soller, 2009). In OTDR, a light pulse is sent through the optical fibre and as the pulse interacts with the optical fiber constituents on a molecular level, secondary electromagnetic waves (light) are generated, a phenomenon referred to as *scattering*. Due to the optical fibre being a non-homogeneous material, the scattering waves propagates in all directions, not just forward (Bao & Chen, 2012). By measuring the reflected, or back-scattered light, the loss distribution along fibre can be characterized along the length of the fibre as the time between the light pulse and back-scattered light is recorded (Güemes & Soller, 2009).

The scattered electromagnetic waves in an optical fibre consists of three spectral components, Rayleigh, Brillouin and Raman. The Rayleigh scattering has the highest intensity of the spectral components and the same frequency as the incident light. The frequency is not affected by strain or temperature in the fibre, but the intensity of the back-scattering varies in a stochastic pattern along the fibre, and the pattern does not change over time as the fibre is impervious to external effects such as electric fields or corrosion (Barrias et al., 2016). In contrast, the Brillouin scatter exhibit frequency changes when the fiber is strained or exposed to temperature changes, and the Raman scatter intensity depends on the temperature in the fibre (Bao & Chen, 2012).

Due to the strain and temperature sensitive properties of the Brillouin scatter and temperature sensitive properties of the Raman scatter, DOFS based on the properties of these electromagnetic waves have been extensively developed for structural health monitoring purposes. Sensors based on Raman scatter can only be used for sensing temperature differences in structures, as it is not sensitive to strain differences, and have, e.g., been applied to detect leakages is pipelines. The Brilluoin scatter, however, has received much attention in the last decades for its ability to quantify distributed strain along the fibre. Two commonly used types of interrogation techniques for sensors utilizing the Brillouin scatter are the Brillouin Optical Time Domain Analysis (BOTDA) and Brillouin Optical Time Refectometry (BOTDR). The BOTDA uses two lasers, one laser sends a pulse while the other laser, connected on the other end of the fibre, send a continuous wave that amplifies the Brillouin scattering at certain frequencies which shifts after applying a strain or temperature change (Bao & Chen, 2012). The concept for BOTDR is similar to the OTDR, but the Rayleigh scatter is filtered out.

The gauge length, or distance between points along the fibre, for Brillouin scattering interrogation techniques lies around 10 cm for relatively short sensing ranges of 1 km (Vlachopoulos, 2023). In order to distinguish cracks in concrete, smaller gauge lengths are required which can be facilitated by interrogation of the sensor with optical frequency domain reflectometry (OFDR). Compared to OTDR, in OFDR, a tunable continuous laser beam is sent into the sensor fibre and a reference fibre with a constant rate of wavelength change. The returning Rayleigh scatter is combined with the electromagnetic waves from the reference fibre before the interference fringes of the combined light is recorded. A Fourier transform is used to convert the data into the spatial domain as the frequency of the back-scattered light increases with the length of the fibre (Kreger et al., 2016). As stated previously in this section, the Rayleigh scattering frequency is not affected by mechanical strain or temperature, but as the fibre is externally exposed to strain or temperature changes, the distance to the detector changes. By dividing the Rayleigh back-scattered amplitude into smaller segments along the length of the fibre and applying an inverse Fourier transform on the segment, the strain change in each segment can be quantified by the frequency shift between a reference measurement taken prior

to straining the fibre and a measurement after the strain change. By using the OFDR interrogation technique, sub-millimeter gauge lengths can be reached, however, the maximum sensing range of 100 m is considerably lower than for Brillouin techniques (Kreger et al., 2016).

Compared to discrete measurement techniques, the use of DOFS in structural health monitoring applications allows for a more precise structural analysis due to the continuous strain measurements. In structures and materials where weak zones and eventual damage are unpredictable, e.g., cracking of concrete or ground settlements from excavations, the system offers a wider monitoring coverage, and thus, increases the possibility of detecting damage compared to discrete measurement systems (Villalba & Casas, 2013). In recent years, DOFS have been implemented for several health monitoring purposes, e.g., monitoring of existing buildings adjacent to construction sites (Barrias et al., 2018; Gómez et al., 2020), crack detection in concrete (Berrocal et al., 2021; Brault et al., 2019; Deif et al., 2010) as well as for displacements in tunnel linings (Battista et al., 2015; Mohamad et al., 2012; Monsberger & Lienhart, 2021).

2.3 Finite element modelling of shotcrete tunnel linings

The finite element method (FEM) in structural engineering is widely used for analysis and design in both the industry and in research. Conventional applications of the method in research include, e.g., verification of structural behaviour in experiments, parametric studies and for simulating structures that are unsuitable for laboratory environments. For modelling of inelastic deformations in a quasi-brittle material, such as shotcrete, the choice of constitutive model depends on the analysis purpose and required output. In this research project, the required output is not yet established, however, some promising models have been identified.

A total strain approach, where the sum of elastic, plastic, creep, thermal and shrinkage strains were combined for the analysis, was adopted by Schädlich and Schweiger (2014) and Schütz (2010) for modelling a shotcrete lining. However, different constitutive models were implemented. Schädlich and Schweiger (2014) used a combination of Mohr-Columb and Rankine yield surfaces for compression and tension respectively, while Schütz (2010) utilized the Chen & Chen (Chen & Chen, 1975) criterion and modified Rankine yield surface. In both models, a smeared crack approach was applied for strain localisation in the tensile regime.

An alternative approach for strain localisation, in shotcrete tunnel linings, has been presented by Sjölander et al. (2020). This approach is specifically developed for local loads in jointed hard rock tunnels and has been verified against previously conducted experiments (Fernandez-Delgado et al., 1975; Holmgren, 1987). Furthermore, a spring-damage model is introduced for bond failure

between rock and shotcrete which is lacking in other FE-models developed for shotcrete in clay or soft rock.

2.4 Data driven AI-models for classification and prediction

The use of artificial intelligence (AI) in the research field of structural engineering and structural health monitoring has increased drastically in the last decade (Salehi & Burgueño, 2018; Tapeh & Naser, 2023). A subarea of AI is machine learning models, which are commonly classified into three categories, reinforcement learning, unsupervised learning and supervised learning. Principally, in reinforcement learning, an agent is given a set of choices and depending on the result, it is rewarded and updated. The process is repeated and with enough iterations, the agent is able to make decisions leading to maximum rewards. In unsupervised learning, data is classified based on beforehand unknown attributes, also known as clustering. Lastly, in supervised learning, data is fed to the model and trained to classify or make estimations based on new, similar data.

For identification of loads and prediction of failure, the supervised learning approaches and, more precisely, decision trees and neural networks are most suitable. A representation of a decision tree is shown in Figure 2.1 which consists of nodes and connections between nodes, or branches. In every node a decision, or separation of data, is made based on the training set and two branches link to two new nodes at the next level of the tree. At a specified level or when the data is uniform, no more branches are created and an end node, or leaf, is created. As new data is fed to the model, the data is processed at the nodes and classified or estimated at the leafs (scikit-learn developers, 2024).

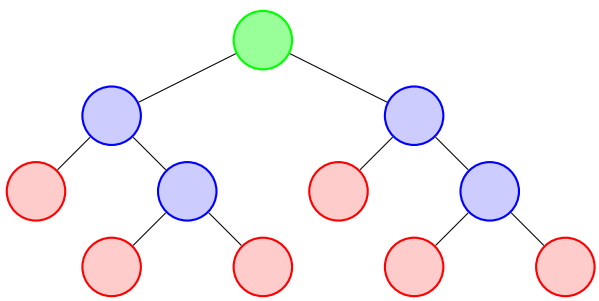

Figure 2.1: A schematic representation of a decision tree. Each node represent a decision and at the leafs, red nodes in the figure, a result is outputted.

A neural network is schematically shown in Figure 2.2 and also consists of nodes arranged in layers, however, the purpose of each node is not as well defined as for decision trees. The number of nodes in each layer and the amount of layers

varies for every model, but in every model an input and an output layer are required. The input layer contain nodes related to data or features in a dataset, and in the output layer, classification or regression nodes are employed to describe the data set. Between the input and output layers, intermediate layers can be added to increase the complexity of the model. The neural network is trained by minimizing an error function based on a predicted value and a target value (Pedregosa et al., 2011).

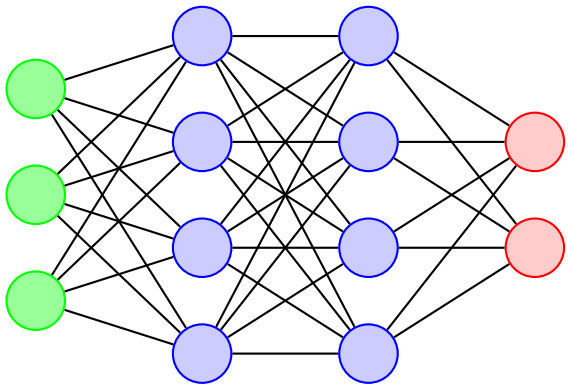

Figure 2.2: Schematic representation of a neural network where green nodes are input nodes and red nodes are output nodes.

Included in the research project is an artificial data generation step in which several FE-models are run with varying input parameters. A straight-forward approach is a parametric study where input data is systematically varied for each parameter. Alternatively, in Vrijdaghs and Verstrynge (2022), stochastic input variables were applied for a bridge case study in over 100 simulations and the results were used for a probabilistic structural analysis. The method allows for a larger range or variation with a smaller computational cost.

Chapter 3

Experiments

In this chapter, the experimental procedures utilized in this thesis are motivated and presented. First, the experimental approach is introduced and experimental choices are discussed, followed by the experimental setup and tests. Two experimental campaigns were undertaken for this work: a preliminary investigation on adhesive bond strength between two layers of concrete (Paper 1) and the main tunnel loading experimental series (Paper 2 and 3) where a lining was cast on top of a concrete substrate and subjected to loads.

3.1 Approach to experiments

As the results of the main experiments are key for the calibration of a FE-model, which in turn will be used to train an AI-model capable of predicting loads and possible failure events, an important discussion and motivation of experimental choices was conducted and described below in this section.

To simulate loads acting on a tunnel lining, load cases presented by Barrett and McCreath (1995) and design recommendations given by the Swedish transport administrations (Trafikverket, 2015), both of which describe rock block loads and distributed loose rock masses as typical loads on tunnel linings, were implemented. The rock block load was simulated as a concrete cone cast into the substrate concrete and a lifting bag was used to replicate the load condition for a loose rock mass.

A notable material choice for the main tunnel load specimens is the substitution of rock and shotcrete. Instead of a rock substrate, concrete is used to improve control of material and geometrical properties. It allows for the casting of centrally placed cones, variation of surface treatments and reduce the risk of substrate failure due to imperfections or faults in rock. A similar reasoning was used for the shotcrete substitution to cast FRC. However, a concrete recipe similar to what is used for shotcrete in tunnel applications was used in the experiment and a small variation in mechanical properties between shotcrete and FRC is expected. Furthermore, compared to a sprayed concrete

layer, the layer thickness of a cast FRC can be better controlled and the risk of breaking optical fibre cables is minimized.

By substituting the materials, the maximum load reached in the experiments may vary when compared to a similar real tunnel case. However, the aim of the experiments is to investigate the lining behaviour through strain patterns when loaded by rock blocks or loose rock material. Even though the strain magnitude measured in the experiments may differ from the magnitudes measured in a real tunnel, strain patterns indicating loads and failure modes can be compared to those of a real tunnel. Moreover, with increased control achieved by the material substitutions, deviation in results between specimens can with higher certainty be attributed to the varied factors, rather than variations in geometry and material properties.

In real tunnels, the bond is usually tested on site by drilling several cores, after the shotcrete has hardened, and loading them in tension. In addition to varying bond strengths, the failure interface of the cores varies between failure in the shotcrete, rock or a combination of the two materials. From the preliminary bond strength experiment presented Paper 1, it was concluded from the literature that a hydro-demolished surface yields around 2 MPa bond strength and mixed failure interface between the two concrete layers. The experiment for exploring the bond properties between two layers of concrete was carried out prior to the main tunnel load experiments and aimed to characterize a low non-zero bond with a failure interface between two layers of concrete.

In addition to the load condition and bond strength, lining thickness and load size were included as factors in the main tunnel load experiment and were chosen based on preliminary modelling results presented in Jansson et al. (2022). Other considered factors were the bolt spacing and total specimen size which only affected the load-displacement behaviour after the initial peak load was reached. As the goal of the project is to show how an AI-algorithm can detect loads and predict eventual failure modes, factors influencing the early behaviour of the lining were therefore prioritized in the experimental design.

3.2 Preliminary tests: tensile bond strength

To investigate the bond between two layers of concrete, four 300 x 300 mm^2 squared concrete slabs with 75 mm thickness were cast and, after hardening for 28 days, the surface of three slabs was ground while the surface of the fourth slab was jackhammered. Subsequently, 100 g of 0-2 mm sand was distributed evenly on one of the ground slabs and 1 cm deep free water was poured on another. After applying the surface treatments, another equally thick layer, 75 mm, was cast on top of each slab. After 30 days of hardening, four cores with 100 mm diameter were drilled from each square slab, and each core was tested in tension as shown in Figure 3.1. The tests were displacement controlled and

one side of the specimens was monitored with digital image correlation (DIC). The maximum load was monitored and the bond stress was determined as force divided by the core sectional area.

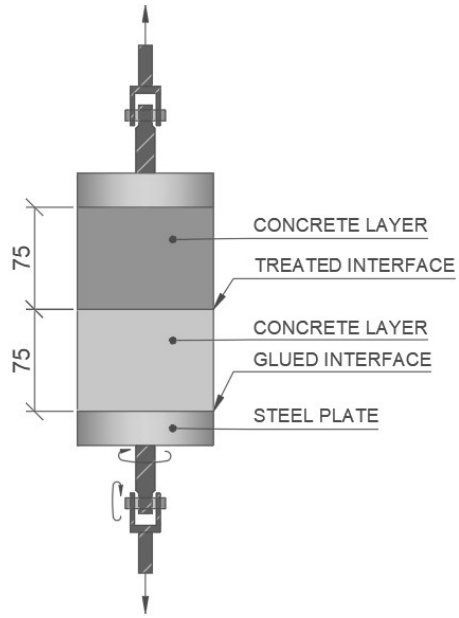

Figure 3.1: Specimen layout and connection setup to the testing machine.

3.3 Main experimental program: Tunnel load

For the experiments simulating tunnel loads on linings, a full factorial design with four factors and two levels for each factor was implemented, resulting in 16 specimens. The investigated factors were load condition, load size, thickness of lining and bond conditions between the lining and the substrate. In Table 3.1, the nomenclature is given for all specimens and each factor is explained below in this section.

The specimens consisted of two separately cast concrete layers with a symmetric octagonal geometry with 1.8 m between parallel sides. The setup is shown in Figure 3.2. The bottom, substrate concrete layer, cast at two occasion with 7 days in between, was 300 mm thick and the top fibre reinforced concrete (FRC) layer thickness, cast 57 days after the substrate slabs, was either 50 mm or 100 mm. The second factor is the two load application methods. For the first load application method, lifting bags were cast in between the two concrete layers and inflated to simulate loose rock material loading the lining. For the second, concrete cones were cast centrally in the substrate concrete layer and pushed through the top FRC layer. Furthermore, the size of the cones and lifting bags were varied as a factor in the factorial design between 0.144 m^2

Table 3.1: Nomenclature for all specimens in the main experimental series and how the specimens correlate to the factors. Underlined letters or numbers in the factor names are used in the specimen nomenclature.

			Surface treatment	
			Ground	Hydro
Load condition Cone - Bag	Load Size Large - Small	Thickness 50-100	CS50G CS100G	CS50H CS100H
		Thickness 50-100	CL50G CL100G	CL50H CL100H
	Load Size Large - Small	Thickness 50-100	BS50G BS100G	BS50H BS100H
		Thickness 50-100	BL50G BL100G	BL50H BL100H

and 0.436 m^2. The last factor in the design is the surface treatment of the substrate slab prior to the top FRC layer casting. The surfaces were either ground or hydro-demolished to vary the bond properties between the concrete layers.

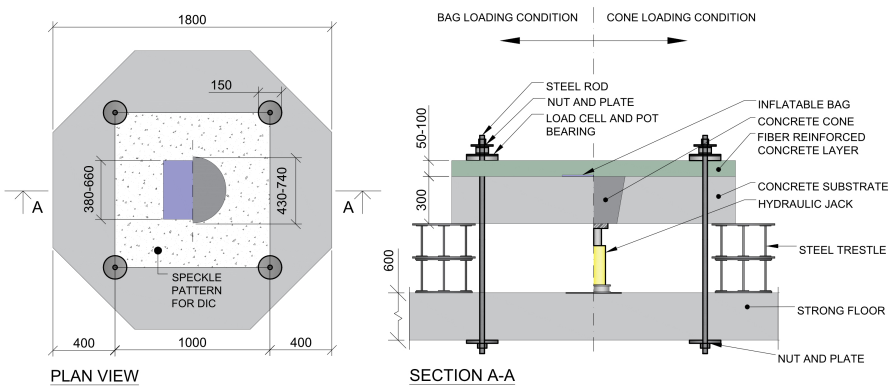

(a) (b)

Figure 3.2: Geometry and layout of experimental specimens. a) Plan view of the specimen with right side for cone loading condition and left side for bag loading condition b) Cross-section of the specimens. The right half shows the geometry for the cone loading condition and the left half shows the bag loading condition. All measurements in mm.

In the top FRC layer of each specimen, optical fibre cables were installed in two layers and two directions. The cables were mounted and tightened in drilled holes in the formwork prior to casting, and by using CNC-machined plywood boards, the cables were placed in a serpentine pattern to cover more of the

specimens in a single cable. During testing, the cables were connected to a Luna ODISI 6108 interrogator, measuring at 6.25 Hz and with 5.2 mm gauge length. The installation of DOFS prior to the casting of the top layer is shown in Figure 3.3

(a) (b)

Figure 3.3: Cable arrangement (blue cables) for a) bag-loaded specimens and b) cone-loaded specimens prior to casting of the top FRC layer.

In addition to the DOFS measurements, a region of the top surface of each specimen was painted white with a stochastic black dotted pattern and continuously photographed with two Aramis 12M cameras during the test at 0.5 Hz. The pictures were later post-processed using digital image correlation (DIC), resulting in a displacement field at the surface of the specimens. Further, for the cone loaded-specimens, three LVDTs were glued to the substrate slab and measured the relative displacement of the cone during testing. Additionally, a load cell was connected to the hydraulic jack. Conversely, in the bag-loaded specimens, the pressure in the bags was measured using a pressure gauge and the displacement was calculated using the DIC.

Displacement control of the hydraulic jack was implemented for the cone-loaded specimens starting at 0.5 mm/min and increased to 2 mm/min after initial failure was reached. For the bag-loaded specimens, in order to avoid over pressurizing and eventual accidental failures, the central 300 bar hydraulic system was connected to a double cylinder setup which decreased the maximum pressure to 26.5 bar. During testing, the double cylinder system was displacement controlled, resulting in a constant increase of oil volume in the bag at 0.213 litres per minute. The double cylinder system also had to be refilled during testing, and consequentially, the test was paused during refill.

In parallel with the idealised loading experiment, material tests for the substrate concrete, the FRC and the bond between the concrete layers were conducted. Concrete cubes were cast during each casting session and tested in compression

according to EN 12390-3:2016. Six cubes were cast for the substrate slabs, three at each casting occasion, and four for the FRC top layer. Furthermore, wedge splitting test specimens were prepared for the FRC and tested according to (Brühwiler & Wittmann, 1990). Cores were drilled at the specimen edge in all bag-loaded specimens and tested using the same methodology explained in Paper 1. All material tests were carried out during the week after finalizing the main loading tests.

Chapter 4

Results

Main findings from the three included papers are presented in this chapter.

4.1 Tensile bond strength tests

Results from the preliminary tests for the characterization of bond between two concrete layers are shown in Table 4.1. A non-zero bond was reached in all specimens and the stress did not reach above 1 MPa for any of the ground specimens. Furthermore, the failure occurred in the interface between the concrete layers in all ground specimens, while the jackhammered specimens had mixed failure interfaces.

Table 4.1: Maximum stress reached for each specimen and mean strength for each surface treatment.

Surface treatment	Max stress [MPa]				Mean strength [MPa]
Jackhammered	1.07	1.26	1.22	1.10	1.16
Ground	0.63	0.31	0.27	0.31	0.38
Ground+100g sand	0.41	0.44	0.41	0.41	0.42
Ground+free water	0.82	0.55	0.66	0.69	0.68

The same test was performed for cores taken from the bag-loaded main loading specimens. In Table 4.2, the surface treatment and failure interface, as well as maximum stress and mean stress, reached in the core specimens are shown. In Figure 4.1, the failure interface types are shown. It should be noted that two of the hydro-demolished cores failed in the glued interface to the machine, see Figure3.1. The mean bond strength in the ground specimens reached 2.29 MPa and 2.73 MPa in the hydro-demolished specimens. Compared to the ground specimens shown in Table 4.1, considerably higher bond strength was reached for the ground specimens as seen in Table 4.2.

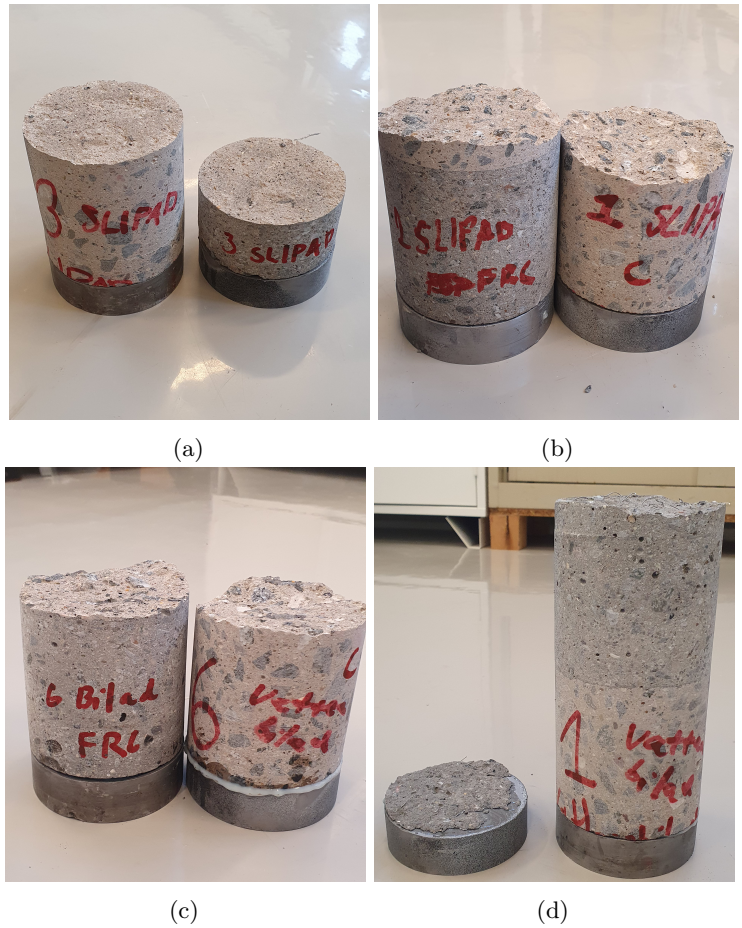

(a) (b)

(c) (d)

Figure 4.1: Failure interfaces for 4 specimens. (a) Bond, (b) substrate, (c) mixed and (d) glued interface

4.2 Main experimental series

For the main experimental series, the global behaviour differed between the two loading conditions, cone-loaded and bag-loaded specimens. The cone-loaded specimens exhibited an initial stiff response with quickly increasing loads at small displacements of the cones, followed by an immediate load loss for ground specimens and a more gradual decrease at increasing displacement for the hydro-demolished specimens. This behaviour is presented in the form of load and displacement curves in Figure 4.2. For cone-loaded specimens, the load measurement is taken from the load cell installed underneath the hydraulic jack and the cone displacement is calculated as the mean between the three LVDTs glued to the substrate slab. Similarly, the behaviour of the bag loaded specimens is shown in Figure 4.3 where the load is calculated as the pressure in the bag multiplied with the bag area and the displacement is extracted from

Table 4.2: Maximum, failure interface and mean stress for drilled cores tested in tension. Specimens failed in the glued interface to the machine are excluded for the mean stress in parenthesis.

Specimen	Treatment	Failure interface	Max stress	Mean stress
BL50H	Hydro	FRC	3.46	2.73 (3.0)
BS50H	Hydro	Glue	2.9	
BS100H	Hydro	Glue	2.0	
BL100H	Hydro	Mixed	2.56	
BL50G	Ground	Bond	3.1	2.29
BS50G	Ground	Bond	2.44	
BS100G	Ground	Substrate	2.12	
BL100G	Ground	Substrate	1.5	

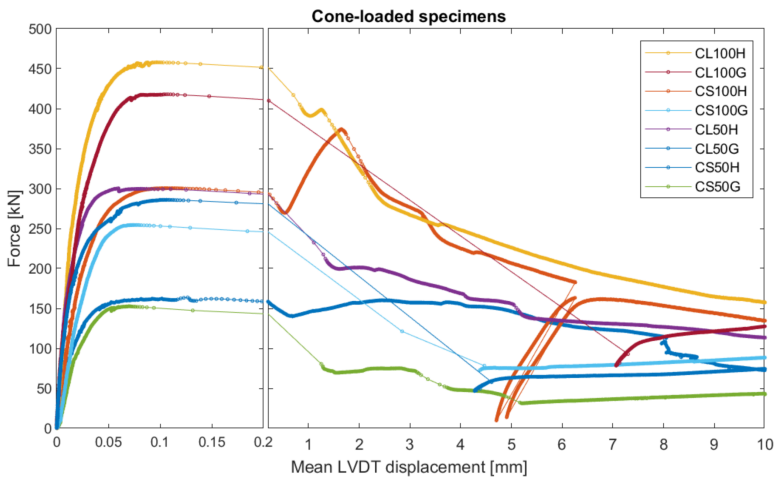

Figure 4.2: Load and displacement curves for the cone-loaded specimens.

the DIC centrally on the specimen. It should be noted that the scale for both displacement and load varies between the sub figures in Figure 4.3. Different scales were chosen in order to highlight the behaviour of each specimen as the magnitude of both load and displacement varied between the specimens.

One of the specimens in Figure 4.2, CS100H, exhibited an increasing load after the initially stiff response and at a later stage, the load is reduced to almost zero at two occasions because of the triggering of a safety mechanism in the testing machine. In Figure 4.3 two specimens, BS100H and BS100G, did not reach failure as the maximum pressure of 26.5 bar was reached and only the initial response is recorded.

Since the optical cables were installed in two layers with a known distance between the cables, the curvature for each DOFS-pair can be calculated using

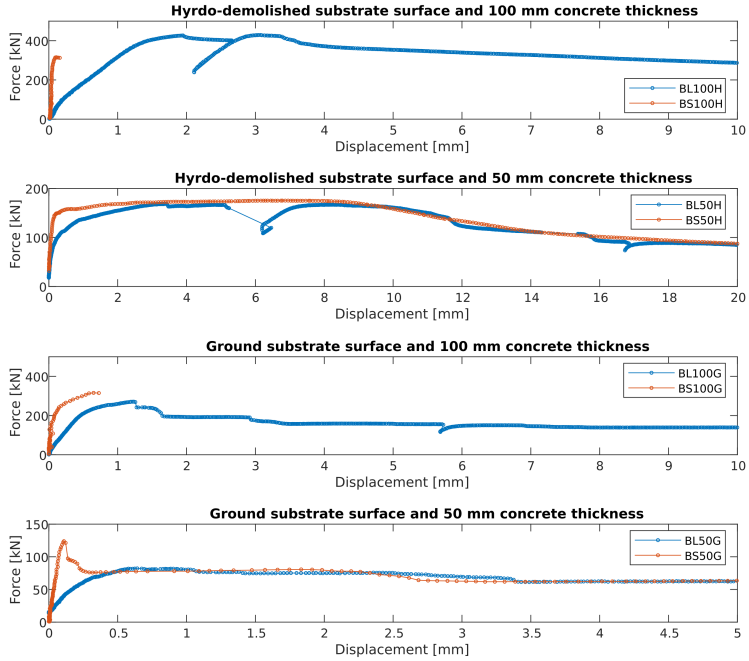

Figure 4.3: Load and displacement curves for the bag-loaded specimens.

equation 4.1, where ε_{top} and ε_{bot} are measured strain in the top and bottom DOFS respectively and z is the distance between the DOFS.

$$\chi = \frac{\varepsilon_{top} - \varepsilon_{bot}}{z} \tag{4.1}$$

In Figure 4.4, results from the DOFS are presented for two specimens, one bag-loaded specimen, BL50H, and one cone-loaded specimen, CL50H. The strain evolution from the start of the test until the peak load for both the top and bottom fibre is presented, as well as the calculated curvature. For both specimens, strains measured in the centrally placed DOFS in one direction is shown and the boundary of the bag or cone is indicated. In the bag loaded specimen, the top fibre is in tension and the bottom fibre is compressed for all load increments up to peak load over the bag. At the bag boundaries tensile strains localize in the bottom fiber and compressive strains is recorded outside the bag boundary for the top fibre. Conversely, both the top and bottom fibre exhibit tensile strains in the cone-loaded specimen and, moreover, the strain magnitude is considerably lower for the cone-loaded specimens compared to the bag-loaded specimen.

After the peak load is reached for the cone-loaded specimens and the load decreased, the strain measurements increase drastically for both layers of fibres.

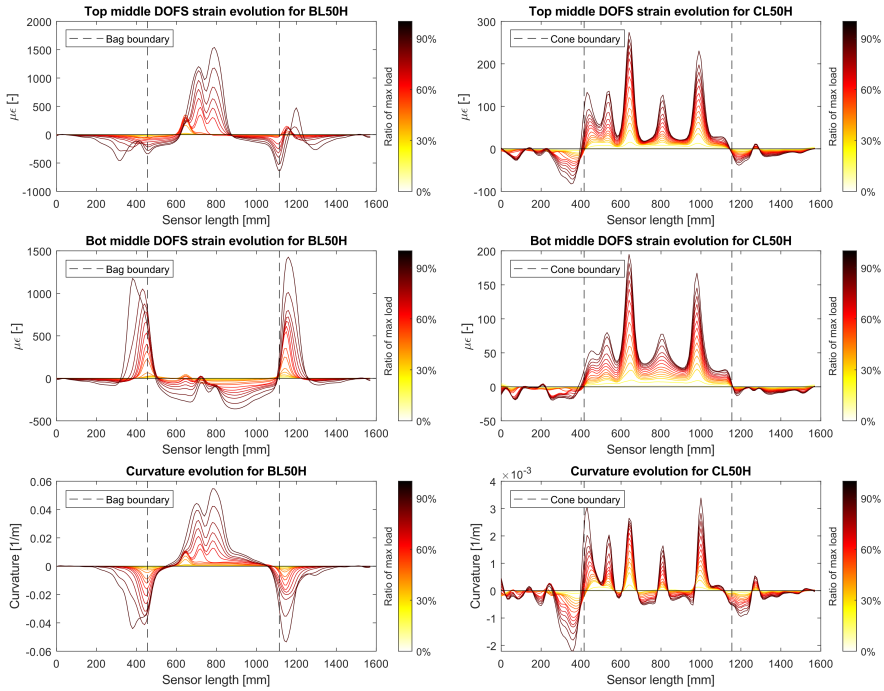

Figure 4.4: Strain and curvature evolution for two specimens, BL50H and CL50H, from 0% to 90% of peak load.

In Figure 4.5, the curvature evolution for all cone-loaded specimens is presented, including curvatures both prior (blue) and after the peak load (red). Each line in the curvature evolution is plotted for a cone displacement shown in Figure 4.2, and the maximum plotted displacement varies as the optical fibre cables broke at different cone displacements. In the ground specimens, positive curvatures are dominating while both positive and negative curvatures are present in the hydro-demolished specimens.

Similarly to Figure 4.5, the curvature evolution for all bag-loaded specimens except BS100G and BS100H which did not reach failure, are shown in Figure 4.6. Compared to the strain evolution in the cone-loaded specimen, the difference of magnitude between curvature prior and after the peak load is smaller for the bag-loaded specimens. Over the lifting bag, larger strains are measured for increased displacements. However, outside the bag boundaries, the negative curvature peaks are further apart after reaching the peak load. Noteworthy is that the distance between the negative peaks are larger for the ground specimens than for the hydro-demolished specimens.

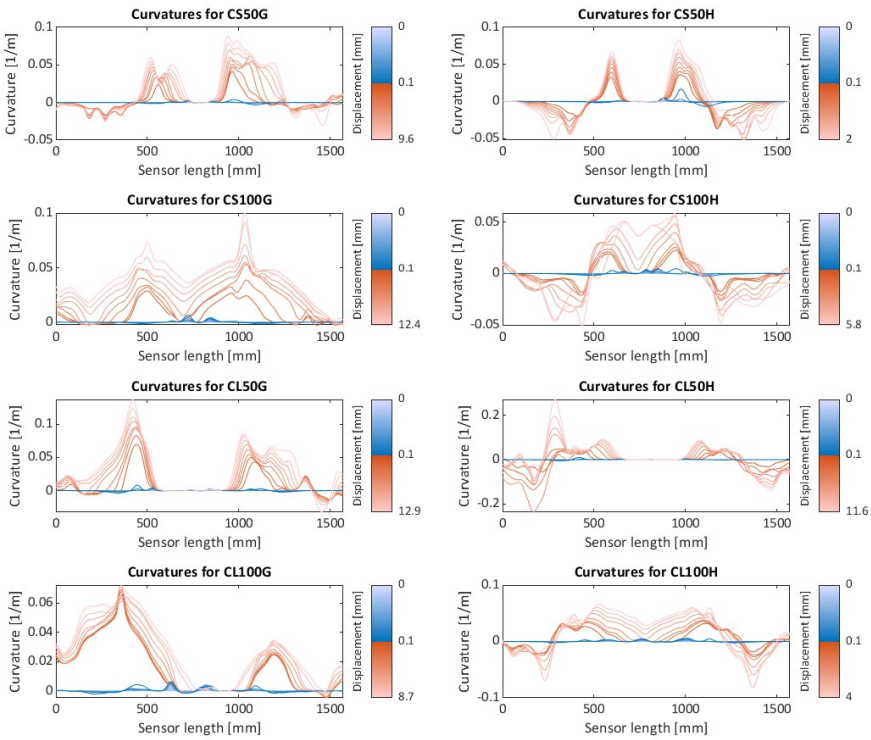

Figure 4.5: Curvature evolution for all cone-loaded specimens. Displacements given in the legends are the cone displacements, also shown in Figure 4.2.

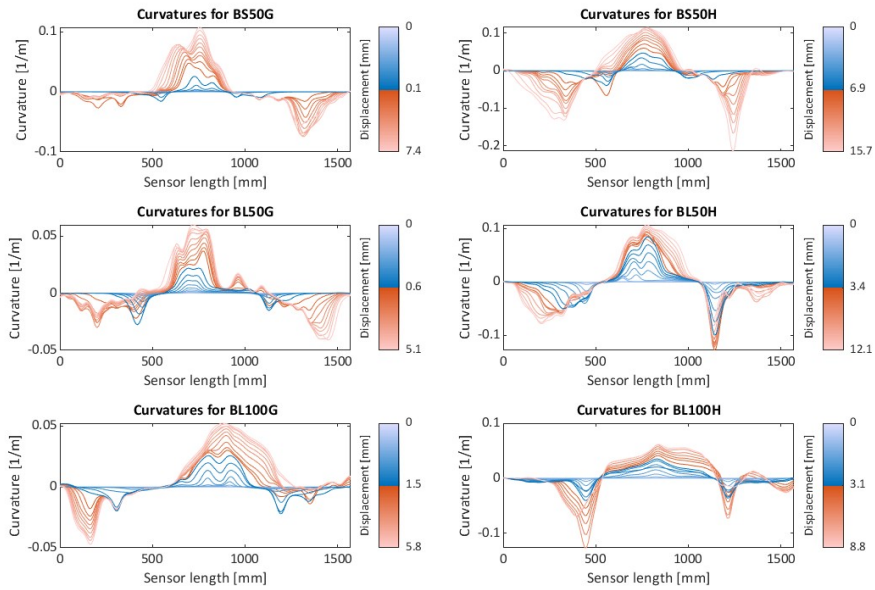

Figure 4.6: Curvature evolution for all bag-loaded specimens. Displacements given in the legends are the top surface displacements measured using DIC, also shown in Figure 4.3.

Chapter 5

Discussion

In this chapter, the experimental results and methods are discussed. The experimental approach in the research project is also discussed as well as implications of the experimental results on future research within the research project.

5.1 Distributed optical fibre sensor resolution

In the main experiments, the applied technique for interrogating the DOFS, OFDR for Rayleigh component back-scatter, had a gauge length of 5.2 mm. This resolution allows for detection of performance indicators, such as cracks, and other strain localisation effects. Other systems, such as BOTDR or BOTDA, can record strains at far longer ranges that would allow for easier installation and fewer connection points of the sensors. However, the maximum resolution for these techniques, as of yet, is around 100 mm (Vlachopoulos, 2023). In Figure 5.1, longer gauge lengths have been simulated by averaging the measured strain over the new gauge lengths for one strain measurement in specimens BL50H and CL50H from Figure 4.4. Strains are plotted for both top and bottom layer fibres at 90% of peak load and the curvature is calculated for both specimens.

For both specimen, the general strain pattern is captured for all gauge lengths, with negative curvature outside the load boundaries and positive over the loaded area. However, none of the the strain localisation occurring over the cone or at the bag boundaries is captured when using 100 mm or 200 mm gauge lengths. A single localisation of strain can be translated as a crack which, consequentially, cannot be detected using 100 mm gauge lengths or higher. In a real tunnel, crack detection would assist tunnel inspections and could be used to identify eventual leakage or risk of corrosion of fibre reinforcement. However, for identifying loads and predicting failure in a machine learning application, the required gauge length should be investigated as longer gauges would allow for combinations with other monitoring systems.

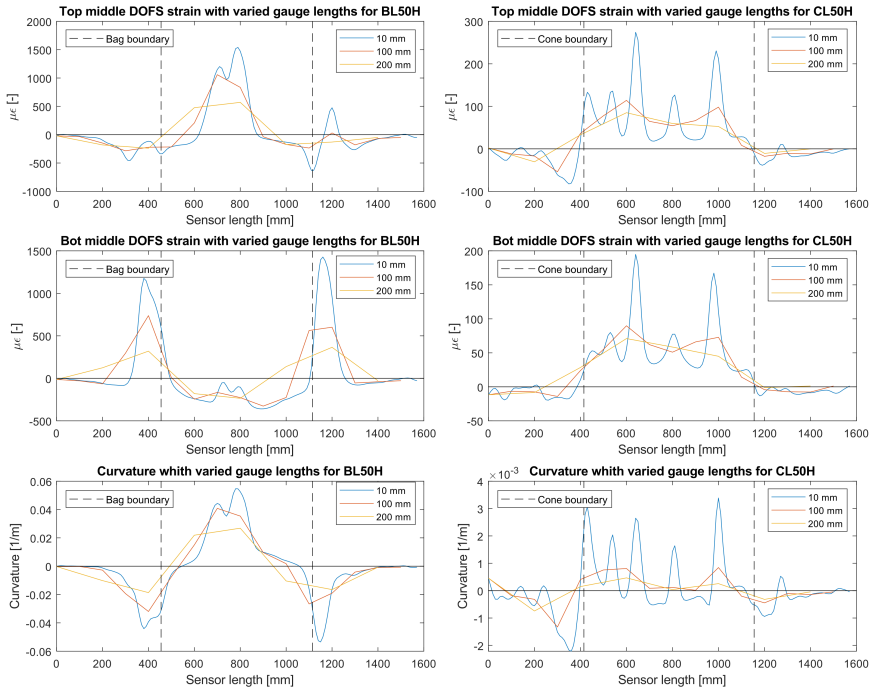

Figure 5.1: Varying gauge lengths for one measurement taken for specimens BL50H and CL50H.

A blasted tunnel in jointed hard rock has inherently an irregular rock surface and, consequently, the sprayed shotcrete thickness will vary along the rock surface. To install optical fibres at a set distance from the rock or concrete edge, as done in this experiment, will require further development of installation techniques and possibly a supporting structure for the optical cables. Alternatively, further development could be invested in developing a method or technique to fix the distance between the two fibres. However, by fixing the distance between two sensors but not the distance to shotcrete edge or rock surface, the most useful result is the curvature as it can be calculated regardless of its position in the lining thickness. In the later stages of the research project, the input required for identifying load types and predicting failure should be investigated.

5.2 Bond behaviour

The low non-zero bond strength conditions achieved in the preliminary tests were not successfully reproduced when applied to the main tunnel load specimens. As described in Table 4.2, a mean tensile bond strength of 2.29 MPa was reached for specimens with ground surface treatments, compared to 2.73 MPa for the hydro-demolished specimens. However, the failure interface varied between the two surface treatments in the core tests, and a variation of strain

patterns were reached in the main tunnel loading experiments. The difference in bond behavior could also be seen in the main load experiments. As concluded in Paper 2, the hydro-demolished bag-loaded specimens both exhibited higher peak loads and mobilized more strain along the DOFS. Moreover, looking at Figure 4.6, the distance between negative curvature peaks after the peak load are smaller for hydro-demolished specimens due to higher moment resistance capacity for hydro-demolished specimens, also described in Paper 2. Furthermore, as seen in Figure 4.5, the bond partially remains intact in the hydro-demolished specimens while total delamination occurs in the ground specimens, which explains the gradual load decrease for hydro-demolished specimens and instant load drop for ground specimens seen in Figure 4.2.

5.3 Strain response at bond failure

Prior to the bond failure, peak load in Figures 4.2 and 4.3, the curvature magnitude in cone-loaded specimens is 10 times smaller than in bag-loaded specimens. As the bond fails in the specimens, the same magnitude levels are reached for both load types as seen in Figure 4.5 and 4.6. The failure process also differ between the load types, the bag-loaded specimens show a ductile behaviour where the strain continuously increased after the bond failure, while the cone-loaded specimens exhibited a sudden increase of strain magnitude.

To identify the bond failure in the bag-loaded specimens, the most obvious indication is the increased distance between negative curvature peaks outside the bag boundaries. Conversely, in the cone-loaded specimens, the bond failure is identified by a distinct increase of strain magnitude both over the loaded area and beyond the cone boundaries. In a tunnel application, where strains in tunnel sections are continuously monitored, the bond failure for both loading types could be detected and the tunnel evacuated followed by proper reinforcement of the section if required after analysis. However, identification of loads and potential failures prior to the bond failure would enable timely measures for securing the safety of the tunnels while larger reparation works and tunnel downtime can be avoided.

5.4 Load type identification

The strain patterns are clearly different between the the load types, see Figure 4.4 and the difference can easily be distinguished. In paper 2, two models were introduced for describing the lining behaviour for both load conditions based on the performance indicators such as crack identification and strain patterns. For the cone-loaded specimens, a strut-and-tie approach was used, which proved suitable to explain the formation of tensile strains in the lining sections and the quick bond failure for all specimens. The lining behaviour in the bag-loaded specimens was described with a fixed-end beam model where the beam is assumed to be uniformly loaded, i.e. by the bag, and the fixed ends corresponds to the intact bond between lining and substrate beyond the

bag boundaries. The model explain both the strain localisation in the bottom fibres at the bag boundary and the curvature over the bag.

However, in a real tunnel lining application, the geometry of the load will differ and a combination of the loads might occur. Considering that the strain measurements from DOFS corresponds to total strain, in addition to the mechanical strain originated by the load, additional strains coming from other effects such as, tunnel convergence, temperature differences, concrete shrinkage or creep will be captured. Furthermore, the position of the optical cable in relation to the load will be a prior unknown. Hence, to differentiate strains caused by loads acting on a lining from the total strain measured, further research focused on characterizing strain from other sources is required. However, by applying a machine learning algorithm, trained on data generated through FE-models including additional parameters, a real time approximation of load type and magnitude may be achieved.

Furthermore, for either load type, no indication of failure, except for the strain and curvature magnitude, can be identified in the strain pattern evolution prior to the failure. However, the strain and curvature magnitude prior to the bond failure differ depending on the load type, which is why a predictive algorithm should be separately developed for each load type.

5.5 Future modelling

The next step in the research project is to investigate an appropriate FE-model for the main load experiment and calibrate it to the experiments. Key elements in the model for accurately capturing strain localisations in the DOFS are the top FRC layer and the bond. The input parameters for the FRC top layer will be derived from the conducted wedge splitting tests and modelled using a smeared crack approach or a stiffness reducing damage model. As concluded in Paper 2, the shear component in the bond influence the failure propagation and must be properly modelled, e.g., using a discrete crack interface, stiffness reducing damage model or a Coulomb friction model. Important, however, during the development of the FE-model, the features required for the machine learning model should also be investigated. As discussed in section 5.1, detecting loads with a lower sensor resolution will decrease both computational time for generating data and allow for applying the method to more types of sensors. However, the quality of the machine learning model predictions must be ensured.

For the AI- implementation part of the project, the type of performance indicators that will be most influential to the model precision and learning rate must also be evaluated, for instance by using engineered features, e.g., curvature, max strain or distance between peaks. Furthermore, the future use of the machine learning model in a real tunnel should be further studied considering precision and responsibility. Eventual results from the model used

for decision making should be verified using other monitoring instrument and human judgement.

Chapter 6

Conclusions and further research

The purpose of the presented thesis was to experimentally identify strain patterns in hard rock shotcrete tunnel linings subjected to local rock block or loose rock material loads using DOFS. Furthermore, the thesis aimed to contextualize the experimental work in the research project and discuss future application of FE and AI models. Based on this, the following conclusions can be drawn.

- Distributed optical fibre sensors are well suited to identify local loads of rock blocks or loose rock material in shotcrete tunnel linings as strain patterns can be distinguished even at low load magnitudes. The high resolution of DOFS used in the experiments captured strain localisations and performance indicators for both load cases.
- Certain aspects of the global behaviour and performance indicators could also be identified using simulated lower resolution DOFS. Consequently, the possibility of utilizing other techniques should be investigated.
- The bond strength reached in the preliminary tests was not reproduced in the main experiments. However, significant variations in the structural behaviour were still captured, where the hydro-demolished bag-loaded specimens showed an increased load capacity compared to ground bag-loaded specimens. Furthermore, after failure, the hydro-demolished cone-loaded specimens exhibited a larger residual capacity and ductility compared to their ground counterparts. The analysis of the main experiments showed that this difference was caused by a higher shear resistance for the hydro-demolished specimens.

For the continuation of the research project, key research issues have been identified and listed below.

- Prior to generating a database, a preliminary investigation of which features are relevant for the development of an AI-model, as well as the

required resolution of strain data from the FE-model, should be carried out. The purpose of the investigation is to understand at which resolution a load in a tunnel lining can be detected and the amount of data that is required to train a trustworthy AI-model.

- Based on the analysis of the experimental results, it is argued that implementing two separate AI-models for the task of identification and failure prediction could be beneficial for increased accuracy. For predicting the failure, a model trained on the specific load type will likely yield more exact results than a combined model.

- To distinguish load induced strains from the measured total strain in a real tunnel, further experimental work for quantifying shrinkage, creep and temperature induced strains are necessary.

- From the analysis of the main experiments, it is concluded that the lining thickness has a large influence on load capacity which in today's design recommendations is not considered. Further research on validating the lining thickness capacity influence and eventual update of design recommendations can improve the use of shotcrete in tunnel linings.

Bibliography

Bao, X., & Chen, L. (2012). Recent progress in distributed fiber optic sensors. *Sensors (Switzerland)*, *12*, 8601–8639. https://doi.org/10.3390/s120708601 (cit. on pp. 10, 11).

Barrett, S. V., & McCreath, D. R. (1995). Shortcrete support design in blocky ground: Towards a deterministic approach. *Tunnelling and Underground Space Technology incorporating Trenchless*, *10*, 79–89. https://doi.org/10.1016/0886-7798(94)00067-U (cit. on pp. 9, 15).

Barrias, A., Casas, J. R., & Villalba, S. (2016). A review of distributed optical fiber sensors for civil engineering applications. *Sensors (Switzerland)*, *16*. https://doi.org/10.3390/s16050748 (cit. on p. 11).

Barrias, A., Rodriguez, G., Casas, J. R., & Villalba, S. (2018). Application of distributed optical fiber sensors for the health monitoring of two real structures in barcelona. *Structure and Infrastructure Engineering*, *14*, 967–985. https://doi.org/10.1080/15732479.2018.1438479 (cit. on p. 12).

Barton, N., Lien, R., & Lunde, J. (1974). Engineering classification of rock masses for the design of tunnel support. *Rock Mechanics*, 189–236. https://doi.org/10.1016/0148-9062(75)91319-4 (cit. on p. 3).

Battista, N. D., Elshafie, M., Soga, K., Williamson, M., Hazelden, G., & Hsu, Y. S. (2015). Strain monitoring using embedded distributed fibre optic sensors in a sprayed concrete tunnel lining during the excavation of cross-passages. *SHMII 2015 - 7th International Conference on Structural Health Monitoring of Intelligent Infrastructure* (cit. on pp. 4, 12).

Bernard, E. S., & Thomas, A. H. (2020). Fibre reinforced sprayed concrete for ground support. *Tunnelling and Underground Space Technology*, *99*, 103302. https://doi.org/10.1016/j.tust.2020.103302 (cit. on p. 9).

Berrocal, C. G., Fernandez, I., & Rempling, R. (2021). Crack monitoring in reinforced concrete beams by distributed optical fiber sensors. *Structure and Infrastructure Engineering*, *17*, 124–139. https://doi.org/10.1080/15732479.2020.1731558 (cit. on pp. 4, 12).

Brault, A., Hoult, N. A., Greenough, T., & Trudeau, I. (2019). Monitoring of beams in an rc building during a load test using distributed sensors. *Journal of Performance of Constructed Facilities*, *33*, 04018096. https://doi.org/10.1061/(asce)cf.1943-5509.0001250 (cit. on p. 12).

Brühwiler, E., & Wittmann, F. H. (1990). The wedge splitting test, a new method of performing stable fracture mechanics tests. *Engineering Fracture Mechanics*, *35*, 117–125. https://doi.org/10.1016/0013-7944(90)90189-N (cit. on p. 20).

Chen, A. C. T., & Chen, W.-F. (1975). Constitutive relations for concrete. *Journal of Engineering Mechanics-asce*, *101*, 465–481. https://api.semanticscholar.org/CorpusID:118047167 (cit. on p. 12).

Deif, A., Martín-Pérez, B., Cousin, B., Zhang, C., Bao, X., & Li, W. (2010). Detection of cracks in a reinforced concrete beam using distributed brillouin fibre sensors. *Smart Materials and Structures*, *19*. https://doi.org/10.1088/0964-1726/19/5/055014 (cit. on p. 12).

Fernandez-Delgado, G., Mahar, J., & Cording, E. (1975). *Shotcrete: Structural testing of thin liners*. Department of Civil Engineering, University of Illinois at Urbana-Champaign. (Cit. on pp. 10, 12).

Gómez, J., Casas, J. R., & Villalba, S. (2020). Structural health monitoring with distributed optical fiber sensors of tunnel lining affected by nearby construction activity. *Automation in Construction*, *117*, 103261. https://doi.org/10.1016/j.autcon.2020.103261 (cit. on p. 12).

Güemes, A., & Soller, B. (2009). Optical fiber distributed sensing: Physical principles and applications. *Structural Health Monitoring 2009: From System Integration to Autonomous Systems - Proceedings of the 7th International Workshop on Structural Health Monitoring, IWSHM 2009*, *1*, 14–20 (cit. on p. 10).

Hahn, T. (1983). *Adhesion of shotcrete to various types of rock surfaces* (Report 55). Rock Engineering Research Foundation. Stockholm, Sweden. (Cit. on p. 10).

Holmgren, J. (1987). Bolt-anchored, steel-fibre-reinforced shotcrete linings. *Tunnelling and Underground Space Technology incorporating Trenchless*, *2*, 319–333. https://doi.org/10.1016/0886-7798(87)90043-5 (cit. on pp. 10, 12).

Hoult, N. A., & Soga, K. (2014). *Sensing solutions for assessing and monitoring tunnels* (Vol. 1). Woodhead Publishing Limited. https://doi.org/10.1533/9781782422433.2.309 (cit. on pp. 3, 10).

Jansson, A., Berrocal, C. G., Fernandez, I., professor, A., & Rempling, R. (2022). Experimental design for shotcrete tunnel lining with distributed optical fibre monitoring. *Proceedings of the XXIV NCR Symposium 2022* (cit. on p. 16).

Kreger, S. T., Rahim, N. A. A., Garg, N., Klute, S. M., Metrey, D. R., Beaty, N., Jeans, J. W., & Gamber, R. (2016). Optical frequency domain reflectometry: Principles and applications in fiber optic sensing. *Fiber Optic Sensors and Applications XIII*, *9852*, 98520T. https://doi.org/10.1117/12.2229057 (cit. on pp. 11, 12).

Malmgren, L., Nordlund, E., & Rolund, S. (2005). Adhesion strength and shrinkage of shotcrete. *Tunnelling and Underground Space Technology*, *20*(1), 33–48. https://doi.org/10.1016/j.tust.2004.05.002 (cit. on p. 10).

Mohamad, H., Soga, K., Bennett, P. J., Mair, R. J., & Lim, C. S. (2012). Monitoring twin tunnel interaction using distributed optical fiber strain measurements. *Journal of Geotechnical and Geoenvironmental Engineering*, *138*, 957–967. https://doi.org/10.1061/(asce)gt.1943-5606.0000656 (cit. on p. 12).

Monsberger, C. M., & Lienhart, W. (2021). Distributed fiber optic shape sensing along shotcrete tunnel linings: Methodology, field applications, and monitoring results. *Journal of Civil Structural Health Monitoring*, *11*, 337–350. https://doi.org/10.1007/s13349-020-00455-8 (cit. on pp. 3, 12).

Palmström, A., & Stille, H. (2015). *Rock engineering (2nd edition)*. ICE Publishing. https://app.knovel.com/hotlink/toc/id:kpREE00021/rock-engineering-2nd/rock-engineering-2nd (cit. on p. 9).

Pedregosa, F., Varoquaux, G., Gramfort, A., Michel, V., Thirion, B., Grisel, O., Blondel, M., Prettenhofer, P., Weiss, R., Dubourg, V., Vanderplas, J., Passos, A., Cournapeau, D., Brucher, M., Perrot, M., & Duchesnay, E. (2011). Scikit-learn: Machine learning in Python. *Journal of Machine Learning Research*, *12*, 2825–2830 (cit. on p. 14).

Salehi, H., & Burgueño, R. (2018). Emerging artificial intelligence methods in structural engineering. *Engineering Structures*, *171*, 170–189. https://doi.org/10.1016/J.ENGSTRUCT.2018.05.084 (cit. on p. 13).

Schädlich, B., & Schweiger, H. F. (2014). A new constitutive model for shotcrete. *Numerical Methods in Geotechnical Engineering - Proceedings of the 8th European Conference on Numerical Methods in Geotechnical Engineering, NUMGE 2014*, *1*, 103–108. https://doi.org/10.1201/b17017-20 (cit. on p. 12).

Schütz, R. (2010). *Numerical modelling of shotcrete in tunnelling*. (Cit. on p. 12).

scikit-learn developers. (2024). Scikit-learn decision trees. Retrieved March 22, 2024, from https://scikit-learn.org/stable/modules/tree.html#decision-trees (cit. on p. 13).

Sjölander, A. (2020). *Structural behaviour of shotcrete in hard rock tunnels*. https://doi.org/10.13140/RG.2.2.34367.12965 (cit. on p. 3).

Sjölander, A., Hellgren, R., Malm, R., & Ansell, A. (2020). Verification of failure mechanisms and design philosophy for a bolt-anchored and fibre-reinforced shotcrete lining. *Engineering Failure Analysis*, *116*, 104741. https://doi.org/10.1016/j.engfailanal.2020.104741 (cit. on p. 12).

Tapeh, A. T. G., & Naser, M. Z. (2023, January). *Artificial intelligence, machine learning, and deep learning in structural engineering: A scientometrics review of trends and best practices*. https://doi.org/10.1007/s11831-022-09793-w (cit. on p. 13).

Trafikverket. (2015). *Projektering av bergkonstruktioner 2014:144*. https://trafikverket.ineko.se/Files/sv-SE/11641/Ineko.Product.RelatedFiles/2014_144_Projektering_av_bergkonstruktioner_handbok.pdf (cit. on pp. 3, 9, 15).

Villalba, S., & Casas, J. R. (2013). Application of optical fiber distributed sensing to health monitoring of concrete structures. *Mechanical Systems and Signal Processing*, *39*, 441–451. https://doi.org/10.1016/j.ymssp.2012.01.027 (cit. on p. 12).

Vlachopoulos, N. (2023). The use of fiber optics for ground and tunnel support monitoring – two decades of lessons learned. *Expanding Underground - Knowledge and Passion to Make a Positive Impact on the World-Proceedings of the ITA-AITES World Tunnel Congress, WTC 2023*, 2336–2344. https://doi.org/10.1201/9781003348030-281 (cit. on pp. 11, 29).

Vrijdaghs, R., & Verstrynge, E. (2022). Probabilistic structural analysis of a real-life corroding concrete bridge girder incorporating stochastic material and damage variables in a finite element approach. *Engineering Structures*, *254*, 113831. https://doi.org/10.1016/J.ENGSTRUCT.2021.113831 (cit. on p. 14).